Article

Effects of Quantum Confinement on Thermodynamic Properties of Ideal Fermion Gases at the Nanoscale

Rivo Herivola Manjakamanana Ravelonjato [1]
https://orcid.org/0009-0006-5658-6153
manjakamanana@yahoo.fr

Ravo Tokiniaina Ranaivoson [1]
https://orcid.org/0000-0003-2233-6106

Raoelina Andriambololona [1]
https://orcid.org/0000-0001-5498-1068

Naivo Rabesiranana [1, 2]
https://orcid.org/0000-0003-0131-9016

Charles Oyverné Randriamaholisoa [3]
https://orcid.org/0009-0008-5522-6257

Wilfrid Chrysante Solofoarisina [1]
https://orcid.org/0009-0005-6370-4608

Malik Maaza [4]
https://orcid.org/0000-0003-3429-509X

Abstract

Quantum confinement in nanoscale systems dramatically alters the thermodynamic behaviour of fermions, with direct implications for nanoelectronics, quantum materials and energy devices. Using a quantum phase space formalism, we derive exact analytical expressions for the thermodynamic properties of an ideal Fermi gas under arbitrary confinement. A central outcome is the introduction of a unified parameter B_u that explicitly links confinement geometry to quantum degeneracy, interpolating smoothly between classical and quantum regimes. This approach predicts an anisotropic pressure tensor, reflecting direction-dependent quantum forces, and a low-temperature heat capacity scaling linearly with temperature, ensuring compliance with the third law of thermodynamics. Classical isotropic behaviour is recovered at high temperatures or large system sizes. Numerical simulations for confined

1 National Institute of Nuclear Sciences and Techniques (INSTN-Madagascar).
2 Department of Physics, Faculty of Sciences, University of Antananarivo, Madagascar.
3 ESSA, University of Antananarivo, Madagascar.
4 iThembaLabs, University of South Africa.

UNISA university of south africa PRESS

Nano-Horizons
Volume 5 | 2026 | #21936 | 12 pages

Nano-Horizons

https://doi.org/10.25159/3005-2602/21936
ISSN 3005-2602 (Online)

electrons (5 nm – 50 nm) at metallic densities confirm that quantum effects dominate at experimentally accessible temperatures. Our results provide a predictive framework for interpreting quantum-confinement phenomena in diverse systems, including 2D perovskites, silicene heterostructures, quantum dot solar cells, and superconducting monolayers, where geometric tuning controls electronic and thermal responses.

Keywords: quantum phase space; anisotropic pressure; shape and size effects; nanoelectronics

1 Introduction

The thermodynamics of fermionic systems under nanoscale confinement is of fundamental importance for nanoelectronics, quantum dots, and nanostructured materials where geometric control dictates device performance [1], [2]. When the system size becomes comparable to the thermal De Broglie wavelength, quantum statistics and boundary effects lead to discrete energy spectra, anisotropic pressure tensors, and modified thermal responses – effects that are critical to designing next-generation nanoscale devices [3]. These effects manifest as pronounced oscillations in thermodynamic and transport properties with varying size and density, as demonstrated in confined degenerate Fermi gases [4].

Although analytical treatments exist for symmetric geometries [5], a unified framework capturing the anisotropic and quantum-size effects for arbitrary confinement has remained a challenge, particularly for real materials where confinement geometry is a tunable experimental parameter [6], [7]. In addition, studies on ultracold Fermi gases in harmonic traps reveal step-like variations in chemical potential and heat capacity due to finite-size effects [8]. The concept of a quantum boundary layer further explains the inhomogeneous equilibrium density distribution in nanocavities, showing universal thickness independent of domain shape [9]. In addition, oscillations in magnetic susceptibility and heat capacity of confined neutral Fermi systems highlight the direct link between confinement geometry and thermodynamic response [10].

Experimental manifestations of quantum-confinement effects are now ubiquitous across material science, with examples spanning photovoltaics (for example, 2D perovskites [11]), 2D materials (for example, silicene heterostructures [12]), high-temperature superconductors (for example, confined FeSe monolayers [13]), quantum dot photodetectors [14], and perovskite nanocrystals for optoelectronic [15] and spintronic [16] applications. In quantum dot (QD) solar cells, the size distribution of *PbS* QDs directly controls the ultrafast charge transfer rate to molecular acceptors by switching the interface band alignment from type I to type II [17]. Similarly, the formation of a two-dimensional electron gas (2DEG) at the surface of Van der Waals ferroelectric $\alpha - In_2Se_3$ is a direct consequence of quantum confinement and strong n-type doping [18]. These diverse studies underscore the necessity of a robust theoretical formalism that directly links geometric parameters to macroscopic thermodynamic and electronic observables.

In this work, we employ a quantum phase space (QPS) formalism to derive exact analytical expressions for key thermodynamic properties – internal energy, anisotropic pressure tensor, and heat capacity – of an ideal Fermi gas under arbitrary nanoscale confinement. Our formalism introduces a central parameter B_u that unifies confinement geometry with quantum degeneracy, naturally incorporating the Fermi energy. This provides a direct link between nanoscale geometry and quantum statistical effects. We demonstrate that pressure becomes a direction-dependent tensor under confinement, while heat capacity exhibits a linear low-temperature regime ($C_v \propto T/T_F$), ensuring compliance with the third law. This linear scaling is analogous to the modified density of states in confined systems observed via spectroscopic techniques in low-dimensional materials [13], [18]. Numerical simulations for confined electrons (5 nm – 50 nm) show that these quantum effects dominate at experimentally accessible temperatures ($10^3K - 10^5K$), relevant for nanoscale electronic components and quantum material design [19], [20].

2 Quantum Phase Space Formalism and Statistical Physics

In the QPS representation, the single-particle Hamiltonian in its mean rest frame is [21], [22]:

$$\boldsymbol{h_A} = \sum_{l=1}^{3}(2\boldsymbol{z}_{Al}^{\dagger}\boldsymbol{z}_{Al} + 1)\frac{\mathcal{B}_{ll}}{m} \tag{1}$$

B_u is the momentum variance in direction l.

where $\boldsymbol{z}_{Al}$ and $\boldsymbol{z}_{Al}^{\dagger}$ are ladder operators related to the coordinates and momenta operators of the particle, l is the index related to space direction ($l = 1,2,3$), m is the mass of the particle A, and B_u is the ground-state momentum variance in the l-th direction of the three dimensional space.

For an ideal Fermi gas, the grand canonical potential is derived as:

$$\Omega = \frac{g_s k_B T}{8}\sum_{j=1}^{\infty}\frac{(-1)^{j+1}\xi^j}{j}\frac{1}{\prod_{l=1}^{3}\sinh\left(j\frac{\beta\mathcal{B}_{ll}}{m}\right)} \tag{2}$$

$\xi = e^{\beta\mu}$ is the fugacity

$n = N/(L_1L_2L_3)$: particle density (m^{-3})

N: total number of particles

$$x_l = j\frac{\beta\mathcal{B}_{ll}}{m}$$

The central result is the unified expression for B_u that interpolates between the classical and quantum degenerate regimes:

$$\mathcal{B}_{ll} = \frac{\hbar}{2L_l}\sqrt{2\pi m k_B T + \pi\hbar^2\left(6\pi^2\frac{n}{g_s}\right)^{\frac{2}{3}}} \tag{3}$$

The detailed derivation of the unified parameter B_u, which interpolates between classical and quantum degenerate regimes, is provided in the Appendix. The second term under the square root corresponds to the Fermi energy per particle, $\epsilon_F = \frac{\hbar^2}{2m}\left(\frac{6\pi^2}{g_s}\right)^{2/3}$, capturing the effect of quantum degeneracy. The parameter B_u effectively encapsulates the competition between thermal energy ($k_B T$) and quantum degeneracy energy (ϵ_F), a competition that is central to the behaviour of confined systems, as seen in the size-dependent charge transfer rates in *PbS* QDs [17] and in the size-tunable optical bandgap and photoresponse of aluminium quantum dots [14].

3 Results

3.1 Direction-Dependent Pressure Tensor

From $P = -\left(\frac{\partial\Omega}{\partial V}\right)_{T,\mu}$, we derive the directional pressure components:

$$P_{kk} = \frac{g_S k_B T}{8V}\sum_{j=1}^{+\infty}\frac{(-1)^{j+1}\xi^j}{\prod_{k=1}^{3} sinh(jx_k)}\left[\, jx_l \coth(jx_l)\right] \tag{4}$$

This directional dependence – demonstrating that under-confinement pressure is not a scalar but a direction-dependent tensor – aligns with the anisotropic pressure distributions predicted for confined ideal gases [5]. However, our expression generalises their result through the parameter B_u, which encapsulates both geometric confinement and quantum degeneracy effects in a single unified form. Each component P_{kk} depends on the confinement geometry through the parameters $x_l \propto 1/L_l$, leading to inherent anisotropy in nanoscale thermodynamics. This formalism can be linked to experimental observations, such as the anisotropic charge transport in oriented 2D perovskite films [11] or the directional-dependent conductivity in emergent materials such as silicene [12]. Furthermore, in magnetically ordered kagome systems, the complex Fermi surface topology – revealed by quantum oscillations – directly manifests direction-dependent transport coefficients, such as the anomalous Hall conductivity, which is intrinsically linked to the Berry curvature distribution in momentum space [23].

Asymptotic behaviours:

- High-temperature/large-size: all directional components converge to the classical isotropic ideal gas pressure, $P_{kk} \to nk_BT$.
- Extreme confinement ($L \to 0$) : the pressure tensor becomes maximally anisotropic – the components along the most confined directions are strongly suppressed, reflecting the dominant role of boundaries.

3.2 Heat Capacity at Constant Volume

The heat capacity $C_v = \left(\frac{\partial U}{\partial T}\right)_{N,V}$ is derived from the internal energy $U = \left(\frac{\partial \Omega}{\partial T}\right)_{V,\mu}$. The exact expression is:

$$C_v = \frac{g_s\, k_B}{8} \sum_{j=1}^{\infty} \frac{(-1)^{j+1}\xi^j}{D^{(j)}} \left\{A_j + \left(\frac{\mu}{T} + \frac{d\mu}{dT}\right) B_j\right\} \tag{5}$$

where:

- $A_j = j \sum_{l=1}^{3} x_l \coth(jx_l) \left[1 - jx_l \coth(jx_l) + \frac{jx_l}{(\sinh(jx_l))^2}\right]$
- $D^{(j)} = \prod_{k=1}^{3} sinh(jx_k)$; $N_0^{(j)} = \sum_{l=1}^{3} x_k \coth\,(jx_k)$; $B_j = j^2 \sum_{l=1}^{3} x_l \coth(jx_l)$
- $\frac{d\mu}{dT} = -\frac{\mu}{T} - k_BT \frac{\sum_{j=1}^{\infty} \frac{j(-1)^{j+1}\xi^j}{D^{(j)}} \left[j \sum_{l=1}^{3} x_l \coth(jx_l) + \frac{j\mu}{k_BT}\right]}{\sum_{j=1}^{\infty} \frac{j^2(-1)^{j+1}\xi^j}{D^{(j)}}}$

➢ Low-temperature limit
- For fermions $T \ll T_F$

$$C_v \approx \frac{\pi^2}{2} Nk_B \frac{T}{T_F} \longrightarrow 0 \text{ (third law compliance)} \tag{6}$$

➢ High-temperature limit
- For both statistics $T \gg T_F$

$$C_v(T \longrightarrow \infty) = \frac{3}{2} Nk_B \text{ (equipartition)} \tag{7}$$

➢ Size dependence under extreme confinement

$$C_v \propto L^{-2} \tag{8}$$

3.3 Numerical Simulation

We simulate an electron gas ($g_s = 2$, $m = 9.11 \times 10^{-31} kg$) confined in a cubic box of side $L = 5\ nm – 50\ nm$, with density $n = 10^{29}\ particles/m^3$. This density is characteristic of a metallic system, closely matching the conduction electron density of aluminium ($n_{Al} \approx 1.8 \times 10^{29}$ m^{-3}), a material of significant interest in nanoplasmonics and nanoelectronics. The corresponding Fermi temperature T_F is therefore intrinsically high (on the order of 10^4 K for $L = 50$ nm), providing a clear energy scale to demonstrate the geometric scaling laws of our model. The condition for observing pronounced quantum-confinement thermodynamics is $\sim T_F$.

Figure 1 shows the following essential physical behaviours:

- Systematic peak shifts with confinement size, following the scaling relation $T_F \propto L^{-2}$. The peak temperature evolves from approximately 10^3 K at $L = 50$ nm to nearly 10^5 K at $L = 5$ nm.
- Peak shape: broad and symmetric, characteristic of a fermionic crossover – not a phase transition. The maximum occurs around $T_F \approx 0.34\, T_F$ with an amplitude of $3.22\, Nk_B$.
- Low-temperature behaviour: a linear temperature dependence, visible as straight-line segments on the log–log plot.

Universal high-temperature convergence to the classical limit of $\frac{3}{2} N k_B$, independent of confinement size.

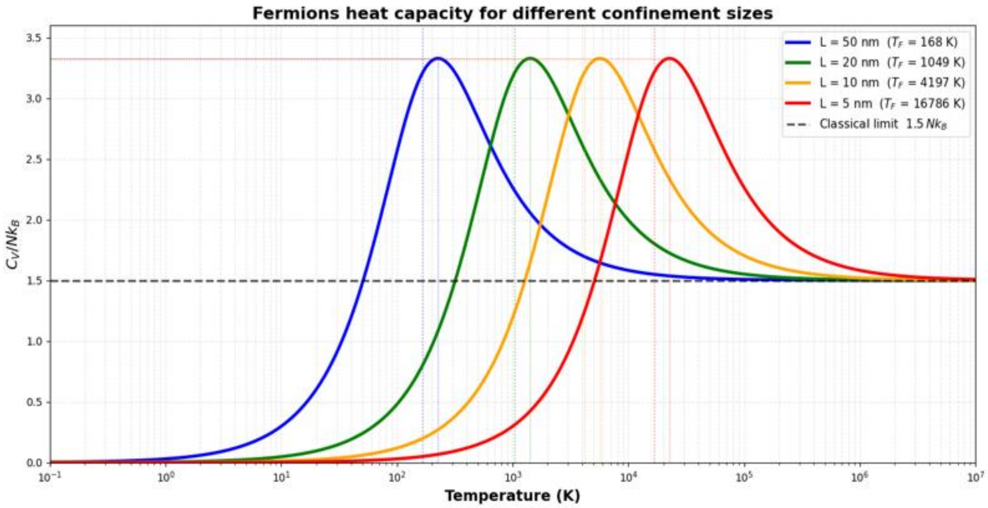

Figure 1: Effects of confinement on fermion gases for dimensions ranging from 50 nm to 5 nm

These observations confirm that fermionic quantum effects become significant at experimentally accessible temperatures (between 10^3 K and 10^5 K) under nanoscale confinement, with the peak position tunable through simple size control.

4 Discussion

Our results indicate that thermodynamics at the nanoscale is fundamentally anisotropic: pressure becomes a tensor whose components are controlled by the confinement geometry via the parameter B_u. This aligns with the idea that geometric and quantum effects in a single confined system can be described by an effective geometric potential, in contrast to Hill's thermodynamics of small systems [6]. This anisotropy is experimentally observable in the directional conductivity of 2D perovskites [11] or in the Fermi surface topology of kagome magnets [23].

The heat capacity C_v exhibits a pronounced peak near $T \sim 0.34\ T_F$, a linear temperature dependence at low temperatures, and scaling $TF \propto L^{-2}$. These features, absent in a confined quantum Maxwell-Boltzmann gas [24], are a direct signature of Fermi-Dirac statistics and energy spectrum quantisation. Crucially, the linear behaviour $C_v \propto T/T_F$ as $T \to 0$ ensures full compliance with the third law of thermodynamics, while at high temperatures C_v converges to the classical equipartition value $\frac{3}{2}Nk_B$, independent of confinement size. Our formalism therefore correctly recovers both the quantum degenerate and classical limits.

Under extreme confinement, the asymptotic behaviour of the pressure tensor and heat capacity requires careful handling of geometric singularities, as discussed for confined fluids [25]. In addition, pure shape effects – independent of size, temperature or density – can be exploited as a control parameter via B_u, a principle demonstrated in quantum shape effect studies [26], [27].

Our numerical simulation for confined electrons confirms the universal scaling $T_F \propto L^{-2}$ quantum effects dominate at experimentally accessible temperatures. However, our model assumes an ideal gas without interactions, It therefore does not directly describe strongly correlated systems (superconductors, kagome magnets) nor defect and interface effects, although these are important in practice [7]. This limitation opens the way for future extensions including interactions and disorder.

5 Conclusions

We have developed a unified QPS formalism for the thermodynamics of an ideal Fermi gas at the nanoscale. From the exact grand canonical potential, we derive closed-form analytical expressions for the unifying parameter B_u, the anisotropic pressure tensor and the heat capacity.

Specifically, we obtain:

- An anisotropic pressure tensor: its components depend on the confinement direction via B_u. At high temperatures or large sizes, the classical isotropic pressure Nk_BT is recovered. Under extreme confinement, the anisotropy is maximal.

- A heat capacity C_v exhibiting:
  - a linear T-dependence at low temperatures, complying with the third law of thermodynamics,
  - a pronounced peak at $T \approx 0.34\ T_F$ with amplitude $\approx 3.22\ Nk_B$,
  - convergence to the classical value $\frac{3}{2}Nk_B$ at high temperatures,
  - a characteristic temperature scaling $T_F \propto L^{-2}$, demonstrated by our simulation for confined electrons.
- A unifying parameter B_u that directly links the nanoscale confinement geometry to the competition between thermal energy k_BT and quantum degeneracy energy ϵ_F, allowing interpolation between the classical and quantum regimes.

These results provide a predictive theoretical framework to interpret and design the thermodynamic properties of fermionic nanosystems. The next challenge is to extend the QPS formalism to interacting and out-of-equilibrium Fermi gases, enabling quantitative modelling of nanostructured materials with strong correlations or complex boundary effects.

6 References

[1] M. Horodecki and J. Oppenheim, "Fundamental limitations for quantum and nanoscale thermodynamics," *Nat. Commun.*, vol. 4, pp. 2059–2065, Jun. 2013, doi: 10.1038/ncomms3059.

[2] A. Aydin and A. Sisman, "Discrete nature of thermodynamics in confined ideal Fermi gases," *Phys. Lett. A.*, vol. 378, pp. 2001–2007, Jul. 2014, doi: 10.1016/j.physleta.2014.05.044.

[3] W.-S. Dai and M. Xie, "Geometry effects in confined space," *Phys. Rev. E.*, vol. 70, p. 016103, Jul. 2004, doi: 10.1103/PhysRevE.70.016103.

[4] A. Aydin and A. Sisman, "Quantum oscillations in confined and degenerate Fermi gases. II. The phase diagram and applications of half-vicinity model," *Phys. Lett. A.*, vol. 382, no. 27, pp. 1813–1817, Jul. 2018, doi: 10.1016/j.physleta.2018.04.053.

[5] H. Pang, W.-S. Dai and M. Xie, "The pressure exerted by a confined ideal gas," *J. Phys. A: Math. Theor.*, vol. 44, p. 365001, Aug. 2011, doi: 10.1088/1751-8113/44/36/365001.

[6] T. L. Hill, "A Different Approach to Nanothermodynamics," *Nano Lett.*, vol. 1, no. 5, pp. 273–275, May 2001, doi: 10.1021/nl010027w.

[7] J. K. Saha and J. Jang, "Saturation Mobility of 100 $cm^2\ V^{-1}\ s^{-1}$ in ZnO Thin-Film Transistors through Quantum Confinement by a Nanoscale In_2O_3 Interlayer Using Spray Pyrolysis," *ACS Nano*, vol. 18, no. 44, pp. 30484–30496, Oct. 2024, doi: 10.1021/acsnano.4c08644.

[8] L. Chen, G. Su and J. Chen, “Ultracold finite-size Fermi gas in a quartic trap,” *Phys. Lett. A*., vol. 376, no. 45, pp. 2908–2910, Oct. 2012, doi: 10.1016/j.physleta.2012.08.017.

[9] C. Firat, A. Sisman and Z. F. Ozturk, “Thermodynamics of gases in nano cavities,” *Energy*, vol. 35, no. 2, pp. 814–819, Feb. 2010, doi: 10.1016/j.energy.2009.08.020.

[10] D. A. Tayurskii and A. R. Minnullin, “Thermodynamic and magnetic properties of the confined neutral Fermi systems,” *Physica B*, vol. 329–333, pp. 152–153, May 2003, doi: 10.1016/S0921-4526(02)01946-4.

[11] X. Dong *et al*., “Quantum Confinement Breaking: Orbital Coupling in 2D Ruddlesden–Popper Perovskites Enables Efficient Solar Cells,” *Adv. Energy Mater*., vol. 13, no. 29, p. 2301006, Aug. 2023, doi: 10.1002/aenm.202301006.

[12] M. Kopciuszynski, A. Stępniak-Dybala, R. Zdyb and M. Krawiec, “Emergent Dirac Fermions in Epitaxial Planar Silicene Heterostructure,” *Nano Lett*., vol. 24, no. 7, pp. 2175–2180, Feb. 2024, doi: 10.1021/acs.nanolett.3c04046.

[13] G. He, Y. Li, Y. Lei, A. Kreisel, B. M. Andersen and J. Wang, “Lateral Quantum Confinement Effect on High-T_c Superconducting FeSe Monolayer,” *Nano Lett*., vol. 24, no. 25, pp. 7654–7661, Jun. 2024, doi: 10.1021/acs.nanolett.4c01435.

[14] H. Wu *et al*., “Quantum-Confinement-Effect-Tuned Cascade AlQDs/β-Ga_2O_3 Heterojunctions for Ultrasensitive Solar-Blind Photodetection and Interference-Resistant Imaging,” *Small*, vol. 21, no. 34, p. 2504173, Aug. 2025, doi: 10.1002/smll.202504173.

[15] M.-R. Amara *et al*., “Spectral Fingerprint of Quantum Confinement in Single $CsPbBr_3$ Nanocrystals,” *Nano Lett*., vol. 23, no. 8, pp. 3607–3613, Apr. 2023, doi: 10.1021/acs.nanolett.3c00793.

[16] M. O. Nestoklon *et al*., “Tailoring the Electron and Hole Landé Factors in Lead Halide Perovskite Nanocrystals by Quantum Confinement and Halide Exchange,” *Nano Lett*., vol. 23, no. 17, pp. 8218–8224, Sep. 2023, doi: 10.1021/acs.nanolett.3c02349.

[17] A. O. El-Ballouli *et al*., “Quantum Confinement-Tunable Ultrafast Charge Transfer at the PbS Quantum Dot and Phenyl-C_{61}-butyric Acid Methyl Ester Interface,” *J. Am. Chem. Soc*., vol. 136, no. 19, pp. 6952–6959, May 2014, doi: 10.1021/ja413254g.

[18] G. Kremer *et al*., “Quantum Confinement and Electronic Structure at the Surface of van der Waals Ferroelectric α-In_2Se_3,” *ACS Nano*, vol. 17, no. 19, pp. 18924–18931, Aug. 2023, doi: 10.1021/acsnano.3c04186.

[19] H.-Y. Ren, Y. Mao, Y.-N. Ren, Q.-F. Sun and L. He, “Tunable Quantum Confinement in Individual Nanoscale Quantum Dots via Interfacial Engineering,” *ACS Nano*, vol. 19, no. 1, pp. 1352–1360, Jan. 2025, doi: 10.1021/acsnano.4c13885.

[20] N. Kumar *et al*., “Quantum Confinement Effect in a Nanoscale Mo/Si Multilayer Structure,” *J. Phys. Chem. C*, vol. 124, no. 32, pp. 17795–17805, Aug. 2020, doi: 10.1021/acs.jpcc.0c03904.

[21] R. T. Ranaivoson, R. Andriambololona, H. Rakotoson and R. H. M. Ravelonjato, “Invariant quadratic operators associated with linear canonical transformations and their eigenstates,” *J. Phys. Commun.*, vol. 6, no. 9, p. 095001, Sept. 2022, doi: 10.1088/2399-6528/ac8520.

[22] R. H. M. Ravelonjato, R. T. Ranaivoson, R. Andriambololona, R. Raboanary, H. Rakotoson and N. Rabesiranana, “Quantum and Relativistic Corrections to Maxwell–Boltzmann Ideal Gas Model from a Quantum Phase Space Approach,” *Found. Phys.*, vol. 53, p. 88, Oct. 2023, doi: 10.1007/s10701-023-00727-5.

[23] B. Wang, *et al*., “Unveiling the Nontrivial Electronic Structures and Fermi Topology of High-Temperature Kagome Ferrimagnet $HoMn_6Sn_6$.” *Nano Lett.*, vol. 24, no. 48, pp. 16031–16038, Nov. 2024, doi: 10.1021/acs.nanolett.4c04411.

[24] T. Markham, J.-Y. Ji and E. D. Held, “Maxwell-Boltzmann statistics of the quantum ideal gas in the canonical ensemble,” *J. Stat. Mech.*, vol. 2020, p. 103103, Oct. 2020, doi: 10.1088/1742-5468/abbac8.

[25] W. Dong, T. Franosch and R. Schilling, “Thermodynamics, statistical mechanics and the vanishing pore width limit of confined fluids,” *Commun. Phys.*, vol. 6, p. 161, Jul. 2023, doi: 10.1038/s42005-023-01255-4.

[26] A. Aydin and A. Sisman, “Quantum shape effects and novel thermodynamic behaviors at nanoscale,” *Phys. Lett. A*., vol. 383, no. 7, pp. 655–665, Feb. 2019, doi: 10.1016/j.physleta.2019.01.009.

[27] C. Kurt, A. Sisman and A. Aydin, “Shape-controlled Bose–Einstein condensation,” *Phys. Scr.*, vol. 100, p. 015289, Jan. 2025, doi: 10.1088/1402-4896/ad9fb2.

Appendix: Determination of the Statistical Variance of Momenta in the Quantum Degenerate Limit

This appendix details the derivation of the statistical variance of momenta B_u for an ideal Fermi gas within the QPS formalism. The parameter is determined by matching the particle density obtained from the exact discrete QPS expression with that from the continuous theory of ideal quantum gases in two distinct limits: the high-temperature (semi-classical) regime and the low-temperature (quantum degenerate) regime.

A.1 High-Temperature Limit (Semi-Classical Regime)

In the high-temperature limit, the following conditions hold:

$\xi = e^{\beta\mu} \ll 1$ and $\beta\mathcal{B}_{ll}/m \ll 1$

$$\Omega_{disc} \cong -\frac{g_s(m)^3\xi}{8(\beta)^4\mathcal{B}_{11}\mathcal{B}_{22}\mathcal{B}_{33}} \tag{A1}$$

This discrete result is equated to the standard semi-classical result obtained from the continuous phase-space integral:

$$\Omega_{cont} \cong -\frac{g_s V}{\hbar^3}\left(\frac{m}{2\pi\beta}\right)^{3/2}\xi \tag{A2}$$

Setting $\Omega_{disc} = \Omega_{cont}$ and solving for $\mathcal{B}_{ll}$ yields the purely thermal contribution:

$$\mathcal{B}_{ll}^{thermal} = \frac{\hbar}{2L_l}\sqrt{2\pi m k_B T} \tag{A3}$$

A.2 Low-Temperature (Quantum Degenerate) Limit ($T \to 0$)

For a Fermi gas at zero temperature, the chemical potential approaches the Fermi energy, $\mu \to \epsilon_F$ which is given by:

$$\epsilon_F = \frac{\hbar^2}{2m}\left(\frac{6\pi^2}{g_s}\right)^{2/3} \tag{A4}$$

In this regime, we match the particle density n

$$n_{disc} = -\frac{1}{V}\left(\frac{\partial\Omega}{\partial\mu}\right)_{T,V} = \frac{1}{8V}\sum_{j=1}^{\infty}\frac{j(-1)^{j+1}\xi^j}{\prod_{l=1}^{3}\sinh(jx_l)} \tag{A5}$$

The standard result from the continuous theory for a fully degenerate Fermi gas is:

$$n_{cont} = \frac{g_s}{6\pi^2}\left(\frac{2m\epsilon_F}{g_s}\right)^{3/2} \tag{A6}$$

Analysing the equality $n_{disc} = n_{cont}$ in the limit $T \rightarrow 0$ allows us to isolate the quantum dominated contribution to B_u. The matching procedure yields:

$$\mathcal{B}_{ll}^{(quant)} = \frac{\hbar}{2L_l}\sqrt{\pi\hbar^2\left(6\pi^2\frac{n}{g_s}\right)^{\frac{2}{3}}} \tag{A7}$$

The term under the square root is proportional to the Fermi energy per particle, ϵ_F.

The results from the two distinct physical limits motivate a unified form for B_u that captures the smooth transition from the classical to the quantum regime.